ACS OMEGA

http://pubs.acs.org/journal/acsodf

Article

Analysis of the Influencing Factors of the Hydroxyl Radical Yield in a Hydrodynamic Cavitation Bubble of a Chitosan Solution Based on a Numerical Simulation

Xiangyu Zhang, Xinfeng Zhu, Yan Cao, Kunming Zhang, Yongchun Huang,* Feng Yang, and Xian'e Ren

Cite This: *ACS Omega* 2021, 6, 3736−3744

Read Online

ACCESS | Metrics & More | Article Recommendations

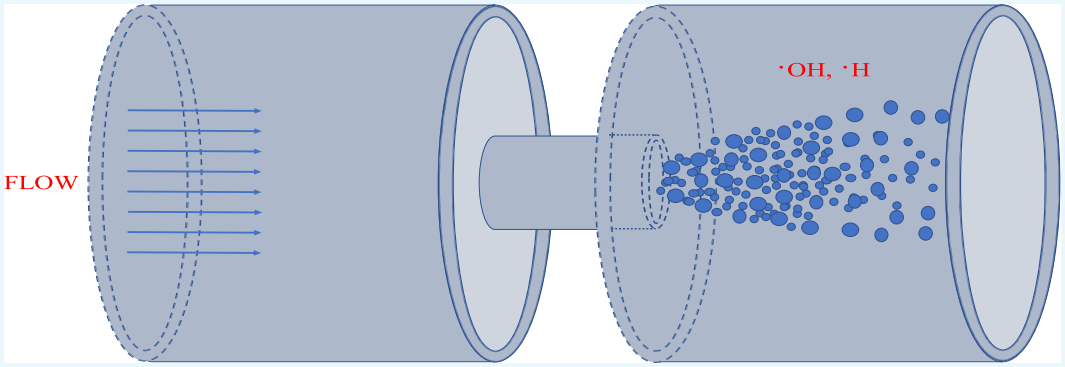

ABSTRACT: In this paper, the hydroxyl radical yield of a cavitation bubble and its influencing factors in the process of chitosan degradation with hydrodynamic cavitation in a single-hole orifice plate was investigated by a numerical simulation method. The hydroxyl radical yield of the cavitation bubble was calculated and analyzed by the Gilmore equation as the dynamic equation combined with the mass transfer equation, heat transfer equation, energy balance equation, and the principle of Gibbs free energy minimization. The influence of geometric parameters of the orifice plate and operating parameters on the formation of hydroxyl radicals was investigated. The results showed that the hydroxyl radicals produced at the moment of cavitation bubble collapse increased with the increase of the initial radius (R_0), upstream inlet pressure (P_1), downstream recovery pressure (P_2), downstream pipe diameter (d_p), and the ratio of the orifice diameter to the pipe diameter (β). The simulation results provide a certain basis for the regulation of hydrodynamic cavitation degradation of chitosan.

1. INTRODUCTION

Chitosan is a natural polymer and can be easily derived by the *N*-deacetylation of chitin. Chitosan can be degraded into oligochitosan with a molecular weight of about 10 000 or less. The oligochitosan has excellent physiological activities, such as cell affinity, nontoxic, antibacterial, anticancer, and biodegradability.[1,2] The degradation methods of chitosan mainly include chemical, enzymatic, and physical methods. Compared with the first two methods, the physical method is more convenient, easy to operate and control, the cost is relatively low, and the degradation products have no pollutants.[3−5] In addition, the biocompatibility of chitosan after physical degradation is not affected, and the degree of deacetylation of the product changes little.[6,7] Therefore, the physical method is a promising route for the degradation of chitosan.

As an efficient and low-energy consumption physical method, hydrodynamic cavitation (HC) has an obvious degradation effect on chitosan.[7−11] The degradation mechanism of HC is that the chemical bonds of chitosan are broken by the mechanical and chemical effects produced during the cavitation bubble collapse. More than 90% of the degradation of chitosan is caused by the chemical effects,[10] which is caused by hydroxyl radicals (•OH).[12−17] Therefore, the key to regulating the HC degradation process is to make the factors affecting the generation of •OH clear.

In the process of HC degradation of chitosan, •OH exists for a short time and can be quickly consumed. Therefore, it is difficult to accurately analyze the effects of cavitation conditions on the production of •OH by experiments. However, the limitations in the experimental process can be solved by a numerical simulation. In this paper, the influence of

Received: November 2, 2020
Accepted: January 14, 2021
Published: January 28, 2021

https://dx.doi.org/10.1021/acsomega.0c05335
ACS Omega 2021, 6, 3736−3744

different factors on the •OH yield of a single cavitation bubble in the chitosan solution was studied by the numerical simulation, which provided the basis for further research on the regulation of the process of HC degradation of chitosan.

2. MATHEMATICAL MODEL

To get closer to the real experimental situation, the discharge coefficient was introduced to calculate the cavitation number. The dynamic model of the cavitation bubble was established using the Gilmore equation,[18] and the yield of •OH was simulated based on the principle of Gibbs free energy minimization.

2.1. Cavitation Number. The cavitation number C_i is the ratio of the two factors that inhibit the formation of liquid cavitation and promote the formation of liquid cavitation, which is defined as[19]

$$C_i = \frac{2 \times (P_2 - P_v)}{\rho \times v_0^2} \tag{1}$$

where P_2 is the downstream recovery pressure of the orifice, P_v is the saturated vapor pressure of the liquid, v_0 is the velocity at the orifice, and ρ is the density of the liquid.

However, the cavitation number depends on the orifice discharge coefficient and the upstream and downstream pressure of the orifice plate in the actual operation of the HC equipment. To get closer to the experimental results, the following empirical formula was used to calculate the cavitation number.[20,21]

$$C_i = \frac{1 - \beta^4}{{C_d}^2} \times \frac{P_2}{P_1} \tag{2}$$

where C_d is the discharge coefficient under cavitation conditions, β is the ratio of the orifice diameter to the pipe diameter. When the pressure difference between P_1 and P_2 is less than 2.8×10^4 Pa and $(P_1 - P_v)/(P_1 - P_2)$ is greater than 1.5, there will be some deviation for C_d. C_d is calculated as follows[22−24]

$$C_d = C_c \times \frac{P_1 - P_v}{P_1 - P_2} \tag{3}$$

$$C_c = 0.62 + 0.38 \times \frac{A_2}{A_1} \tag{4}$$

where C_c is the contraction coefficient, A_2 is the cross-sectional area of the orifice, and A_1 is the cross-sectional area of the pipe. C_{ch} is a choking cavitation number, which can be defined as follows[23,25−27]

$$C_{ch} = 2 \times \left(\frac{A_2}{A_1}\right)^2 \times \left(\frac{A_1}{A_2 \times C_c} - 1\right) \tag{5}$$

When C_i is less than C_{ch}, choking cavitation occurs in the cavitation device, and the cavitation equipment cannot produce an effective cavitation effect.

2.2. Cavitation Bubble Dynamics Equation. This paper makes the following assumptions: (1) The cavitation bubble always keeps a spherical shape during movement. (2) Inside the cavitation bubble is a mixture of water vapor and argon.[12] (3) The temperature and pressure in the cavitation bubble are evenly distributed in space.[28−30] (4) The speed of sound in the chitosan solution is equal to the speed of sound in the aqueous solution due to the extremely low concentration of the chitosan solution. Taking into account the effects of viscosity, surface tension, and compressibility of the solution on the cavitation bubble wall motion process, the Gilmore equation is used to describe the time-dependent variation of the cavitation bubble radius in the flow field downstream of the orifice plate[18,31]

$$\left(1 - \frac{1}{c}\frac{dR}{dt}\right)R\frac{d^2R}{dt^2} + \frac{3}{2}\left(1 - \frac{1}{3c}\frac{dR}{dt}\right)\left(\frac{dR}{dt}\right)^2 = \left(1 + \frac{1}{c}\frac{dR}{dt}\right)H + \frac{R}{c}\left(1 - \frac{1}{c}\frac{dR}{dt}\right)\frac{dH}{dt} \tag{6}$$

$$H = \frac{n(P_t + B)}{(n-1)\rho}\left[\left(\frac{P_R + B}{P_t + B}\right)^{n-1/n} - 1\right] \tag{7}$$

$$c = c_\infty\left(\frac{P_R + B}{P_t + B}\right)^{n-1/2n} \tag{8}$$

where R is the instantaneous radius of the cavitation bubble, c is the local sound velocity in the liquid, H is the enthalpy of the liquid on the wall of the cavitation bubble, c_∞ is the sound velocity in the undisturbed liquid, which is 1480 m/s, n is 7.15, B is 3.05×10^8 Pa, and P_R is the pressure at the cavitation bubble wall, which can be defined as follows

$$P_R = P_i - \frac{2\sigma}{R} - \frac{4\mu}{R}\frac{dR}{dt} \tag{9}$$

where σ is the surface tension coefficient of the liquid, μ is the viscosity coefficient of the liquid, and $_{Pi}$ is the gas pressure inside the cavitation bubble, which can be defined as follows

$$P_i = \frac{N_{tot}(t)kT(t)}{\left[\frac{4\pi}{3}(R^3(t) - h^3)\right]^\gamma} \tag{10}$$

where N_{tot} is the total molecular number of the gas in the cavitation bubble, $h = R_0/8.86$ is the van der Waals hard core radius, determined by the excluded volume of gas molecules, and $\gamma = 1$ is the effective polytropic exponent.[14]

2.3. Heat and Mass Transfer Model of the Cavitation Bubble Wall. High temperature and pressure will be produced at the moment of collapse of the cavitation bubble. The thermal energy and water molecules in the cavitation bubble are transferred and diffused into the surrounding liquid through the cavitation bubble wall boundary layer. The variation of the number of water molecules in the cavitation bubble is described as follows[14,28,29]

$$\frac{dN_w}{dt} = 4\pi R^2 D\frac{n_r - n_w}{l_{diff}} \tag{11}$$

$$l_{diff} = \min\left(\sqrt{\frac{RD}{dR/dt}}, \frac{R}{\pi}\right) \tag{12}$$

where n_r is the number density of water molecules at the cavitation bubble wall, n_w is the actual number density of water molecules in the cavitation bubble, l_{diff} is the thickness of the diffusion boundary layer, and D is the diffusion coefficient of water molecules, which is calculated according to Chapman−Enskog theory. The thermal energy transfer of the cavitation bubble wall is similar to mass transfer, which can be estimated by the following formula[14,28,29]

https://dx.doi.org/10.1021/acsomega.0c05335
ACS Omega 2021, 6, 3736−3744

Table 1. Substances Produced after the Collapse of the Cavitation Bubble

numbering	1	2	3	4	5	6	7	8	9
substance	H_2	O_2	$^{\bullet}OH$	H_2O_2	$^{\bullet}H$	$^{\bullet}HOO$	$^{\bullet}O$	O_3	H_2O

$$\frac{dQ}{dt} = 4\pi R^2 \lambda \frac{T_0 - T}{l_{th}} \tag{13}$$

$$l_{th} = \min\left(\sqrt{\frac{R\chi}{dR/dt}}, \frac{R}{\pi}\right) \tag{14}$$

where λ is the thermal conductivity of the gas mixture in the cavitation bubble, l_{th} is the thermal boundary layer thickness, and χ is the thermal diffusivity.

2.4. In the Cavitation Bubble Energy Balance Model. The region surrounded by the cavitation bubble wall is regarded as an open thermodynamic system. According to the first law of thermodynamics, the energy conservation equation in the cavitation bubble is as follows[14,28,29]

$$\frac{dE}{dt} = \frac{dQ}{dt} - P_i\frac{dV}{dt} + h_w\frac{dN_w}{dt} \tag{15}$$

where E is the internal energy of the gas in the cavitation bubble and $h_w = 4kT_0$ is the enthalpy of water molecules entering the cavitation bubble from the gas−liquid interface.

$$E = \frac{3}{2}N_{Ar}kT + \left(\frac{6}{2} + \sum\left(\frac{\theta_i/T}{e^{\theta_i/T} - 1}\right)\right)N_w kT \tag{16}$$

By substituting eq 11 into eq 10, the change of temperature in the cavitation bubble with time is obtained.

$$\frac{dT}{dt} = \frac{1}{C_v}\frac{dQ}{dt} - \frac{P_i}{C_v}\frac{dV}{dt} + \frac{1}{C_v}\left(4T_0 - 3T - T\sum\left(\frac{\theta_i/T}{e^{\theta_i/T} - 1}\right)\right)\frac{dN_w}{dt}k \tag{17}$$

$$C_v = \frac{3}{2}N_{Ar}k + \left(\frac{6}{2} + \sum\left(\frac{(\theta_i/T)^2 e^{\theta_i/T}}{(e^{\theta_i/T} - 1)^2}\right)\right)N_w k \tag{18}$$

where C_v is the specific heat at the constant volume of the gas in the cavitation bubble and θ is the oscillation characteristic temperature of water molecules, where θ_1 = 2295 K, θ_2 = 5225 K, and θ_3 = 5400 K.

2.5. Reaction Model in the Cavitation Bubble. In the process of cavitation bubble expansion, a large number of water molecules diffuse into the cavitation bubble. When the cavitation bubble wall pressure reaches the Blake threshold, the cavitation bubble shrinks sharply and collapses rapidly. The time scale of the cavitation bubble collapse is much smaller than that of the water molecules diffusing out of the cavitation bubble, so a significant amount of water molecules in the cavitation bubble are trapped and cannot diffuse out of the cavitation bubble.[12,28] The water molecules absorb a lot of energy and decompose under the environment of high temperature and high pressure caused by cavitation collapse. The main products are $^{\bullet}OH$, $^{\bullet}H$, H_2, H_2O_2, $^{\bullet}HOO$, $^{\bullet}O$, O_2, HO_2, and O_3.[13,14,29,32] The main chemical reactions occurring in the cavitation bubble are as follows (M for energy)

$$H_2O + M \rightarrow {}^{\cdot}H + {}^{\cdot}OH + M \tag{19}$$

$${}^{\cdot}H + {}^{\cdot}H \rightarrow H_2 \tag{20}$$

$${}^{\cdot}OH + {}^{\cdot}OH + M \rightarrow H_2O_2 + M \tag{21}$$

$${}^{\cdot}OH + M \rightarrow {}^{\cdot}O + {}^{\cdot}H + M \tag{22}$$

$${}^{\cdot}O + {}^{\cdot}HO_2 + M \rightarrow O_2 + {}^{\cdot}HO + M \tag{23}$$

$${}^{\cdot}H + O_2 + M \rightarrow {}^{\cdot}HO_2 + M \tag{24}$$

$$O_2 + {}^{\cdot}O + M \rightarrow O_3 + M \tag{25}$$

The nine substances considered in this study are the main substances after cavitation bubble collapse, and they are all gaseous at the temperature and pressure of cavitation bubble collapse. Therefore, the total Gibbs free energy of the system can be obtained by adding the Gibbs free energy of each component. The minimum total Gibbs free energy indicates that the system has reached a chemical equilibrium state. The nine substances produced after the collapse of the cavitation bubble are numbered, as shown in Table 1.

The total Gibbs free energy equation of the system is as follows

$$G_{total} = G_{gas}(T, P, n_1, n_2, n_3, n_4, ..., n_9) \tag{26}$$

where G_{gas} is the total Gibbs free energy of the gas phase. Assuming that there are W kinds of elements and N kinds of substances in the reaction system, the element conservation equation of the system is as follows

$$\sum_{i=1}^{N} n_i Y_i = A_Y \ (Y = 1, 2, 3, ..., W) \tag{27}$$

where n_i is the molar mass of substance i, Y_i is the number of atoms of the Y element in substance i, and A_Y is the total molar mass of element Y. Due to the conservation of W kinds of elements, there are a total of W equations.

The above problem can be transformed into solving the extreme value of the total Gibbs free energy equation under the given T, P, and $\sum_{i=1}^{N} n_i Y_i - A_Y = 0$. The Lagrangian multiplier method is the preferred method for solving this extreme value problem, but the accuracy of this method depends on the initial estimated value of the Lagrangian multiplier. The Lagrange multiplier λ_k (k = 1, 2, 3,...,n) is usually introduced to construct the function

$$F = G(T, P, n_1, n_2, ..., n_9) + \sum_{k=1}^{w}\lambda_k\left[\sum_{i=1}^{N} n_i Y_i - A_Y\right] \tag{28}$$

The partial derivatives of n_1, n_2,...,n_9, λ_1, and λ_2 are obtained, respectively, by this function. The simplified nonlinear equations are solved using the fsolve function provided by MATLAB software.

2.6. Simulation Conditions. In this study, an aqueous solution of chitosan was used as the cavitation medium. The viscosity average molecular weight of chitosan was 400 kDa. The effect of different factors, such as upstream inlet pressure (P_1), downstream recovery pressure (P_2), chitosan solution concentration, solution temperature, initial cavitation bubble

https://dx.doi.org/10.1021/acsomega.0c05335
ACS Omega 2021, 6, 3736−3744

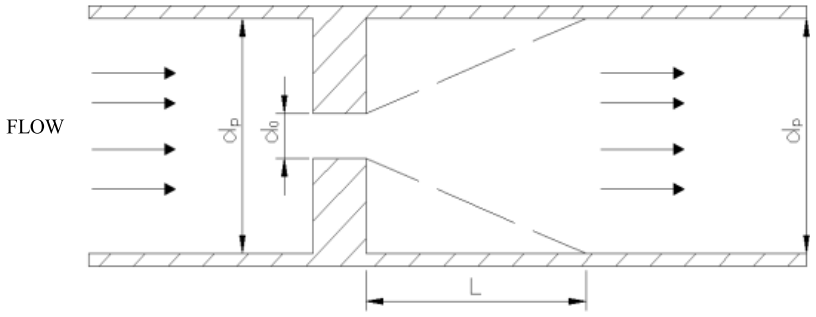

Figure 1. Geometrical sizes of the orifice plate.

radius (R_0), downstream pipeline diameter (d_p), and the ratio of the orifice diameter to the pipe diameter (β), on the yield of •OH and cavitation bubble dynamics was investigated. The initial conditions used for the solution were as follows: $t = 0$, $R = R_0$, $dR/dt = 0$, $N_w = 0$, and $T = T_0$.

2.7. Structure of the Hydrodynamic Cavitation Device. An HC device with a single-hole orifice plate structure was used in this study, as shown in Figure 1. The cross sections of the pipe and the orifice hole were circular. d_p was the pipe diameter, d_0 was the orifice diameter, and L was the length of the pressure recovery zone downstream of the orifice plate.

3. RESULTS AND DISCUSSION

3.1. Effect of the Upstream Inlet Pressure. Under the conditions of T_0 = 303 K, C = 0.2 wt %, R_0 = 100 μm, P_2 = 0.1 MPa, d_0 = 9 mm, and d_p = 25 mm, the influence of the upstream inlet pressure (0.3, 0.35, 0.4, 0.45, and 0.5 MPa) on the •OH yield was investigated. The results are shown in Figure 2 and Table 2.

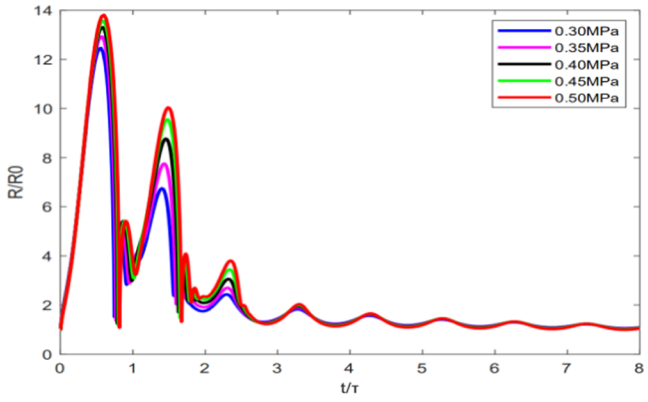

Figure 2. Variation curve of the cavitation bubble radius ratio with dimensionless time under different upstream inlet pressures. (P_1 = 0.3, 0.35, 0.4, 0.45, and 0.5 MPa; T_0 = 303 K; C = 0.2 wt %; R_0 = 100 μm; P_2 = 0.1 MPa; d_0 = 9 mm; and d_p = 25 mm).

The maximum cavitation bubble radius ratio increased slightly as well as the collapse pressure and collapse temperature of the cavitation bubble increased with the increase of the upstream inlet pressure. Furthermore, with the increase of the pressure gradient and turbulence intensity, the cavitation bubble collapse effect was enhanced, so the decomposition rate of water vapor in the cavitation bubble accelerated and the •OH production increased.[33] When the downstream recovery pressure P_2 was 0.1 MPa, the choking

Table 2. Collapse Pressure, Collapse Temperature, Water Molecular Number, and •OH Yield in the Cavitation Bubble under Different Upstream Inlet Pressures

upstream inlet pressure/MPa	collapse pressure/Pa	collapse temperature/K	molecular number of water (N_w)	hydroxyl radical/mol
0.30	1.54×10^6	1305.62	1.18×10^{15}	4.44×10^{-13}
0.35	2.53×10^6	1463.75	1.24×10^{15}	9.35×10^{-13}
0.40	3.74×10^6	1595.55	1.29×10^{15}	1.46×10^{-12}
0.45	5.11×10^6	1707.96	1.32×10^{15}	2.19×10^{-12}
0.50	6.78×10^6	1817.55	1.33×10^{15}	2.89×10^{-12}

cavitation ($C_i < C_{ch}$) occurred in the downstream recovery zone of the orifice plate as the upstream inlet pressure increased to 0.54 MPa. As a result, the cavitation bubble collapse was poor due to the very small value of C_i.[34,35] Therefore, within a certain range, the increase in upstream pressure was conducive to the generation of •OH. This was consistent with the experimental studies.[26,27,33−35]

3.2. Effect of the Downstream Recovery Pressure. Under the conditions of T_0 = 303 K, C = 0.2 wt %, R_0 = 100 μm, P_1 = 1 MPa, d_0 = 9 mm, and d_p = 25 mm, the effect of the downstream recovery pressure (0.2, 0.25, 0.3, 0.35, and 0.4 MPa) on the •OH yield was studied.

Figure 3 and Table 3 show that the maximum cavitation bubble radius ratio increased slightly as well as the collapse pressure and collapse temperature of the cavitation bubble increased with the increase of the downstream recovery pressure. When the upstream inlet pressure remained

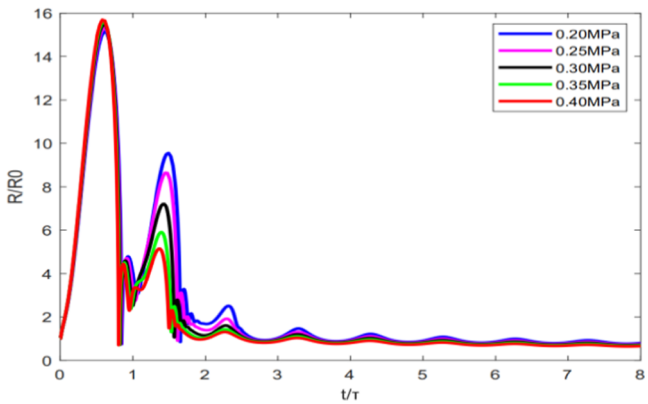

Figure 3. Variation curve of cavitation bubble radius ratio with dimensionless time under different downstream recovery pressures. (P_2 = 0.2, 0.25, 0.3, 0.35, and 0.4 MPa; T_0 = 303 K; C = 0.2 wt %; R_0 = 100 μm; P_1 = 1 MPa; d_0 = 9 mm; d_p = 25 mm).

https://dx.doi.org/10.1021/acsomega.0c05335
ACS Omega 2021, 6, 3736−3744

Table 3. Collapse Pressure, Collapse Temperature, Water Molecular Number, and •OH Yield in the Cavitation Bubble under Different Downstream Recovery Pressures

recovery pressure/MPa	collapse pressure/Pa	collapse temperature/K	molecular number of water (N_w)	hydroxyl radical/mol
0.20	3.13×10^7	2505.57	1.45×10^{15}	9.56×10^{-12}
0.25	3.35×10^7	2536.39	1.52×10^{15}	1.00×10^{-11}
0.30	3.61×10^7	2573.69	1.56×10^{15}	1.04×10^{-11}
0.35	3.89×10^7	2612.37	1.58×10^{15}	1.08×10^{-11}
0.40	4.28×10^7	2665.23	1.59×10^{15}	1.15×10^{-11}

unchanged, the energy dissipation rate per unit mass of the liquid and the pressure loss decreased with the increase of the downstream recovery pressure, so the turbulence frequency and intensity increased. With the increase of the turbulence intensity downstream of the orifice plate, the expansion and collapse of the cavitation bubble became more severe and the decomposition rate of water vapor in the cavitation bubble accelerated. Therefore, the yield of •OH in the cavitation bubble increased when the downstream recovery pressure increased.[21,33]

3.3. Effect of the Chitosan Solution Concentration. Under the conditions of T_0 = 303 K, R_0 = 50 μm, P_1 = 0.5 MPa, P_2 = 0.1 MPa, d_0 = 9 mm, and d_p = 25 mm, the effect of the concentrations of the chitosan solution (0, 0.2, 0.4, and 0.6 wt %) on the •OH yield was studied.

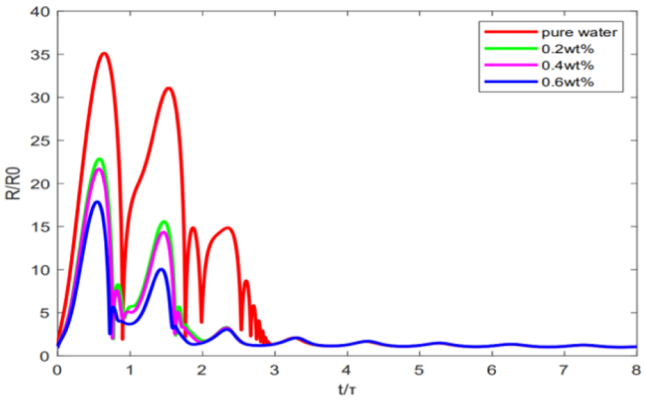

Figure 4. Variation curve of the cavitation bubble radius ratio with dimensionless time at different concentrations. (C = 0, 0.2, 0.4, and 0.6 wt %; T_0 = 303 K; R_0 = 50 μm; P_1 = 0.5 MPa; P_2 = 0.1 MPa; d_0 = 9 mm; and d_p = 25 mm).

Figure 4 and Table 4 show that the maximum bubble radius ratio, collapse temperature, and pressure decreased with the increase of the concentration of the chitosan solution. As the concentration of the chitosan solution increased, the viscosity of the system increased, which caused the increase of the resistance to the formation of the gas core and bubble expansion. Therefore, with the decrease of the maximum radius of the bubble and the cavitation strength, the collapse pressure, collapse temperature, and the production of hydroxyl radicals decreased. Moreover, with the increase of the chitosan concentration, the partial pressure of water vapor and the number of the water molecules entering the bubble from the air interface further decreased. Therefore, the increase of the concentration of the chitosan solution decreased the production of hydroxyl radicals and the degradation effect also decreased, which was consistent with the experimental results.[7]

3.4. Effect of the Solution Temperature. Under the conditions of R_0 = 50 μm, P_1 = 0.5 MPa, P_2 = 0.1 MPa, C = 0.2 wt %, d_0 = 9 mm, and d_p = 25 mm, the influence of the liquid temperature (293, 298, 303, and 308 K) on the •OH yield was investigated. The results are shown in Figure 5 and Table 5.

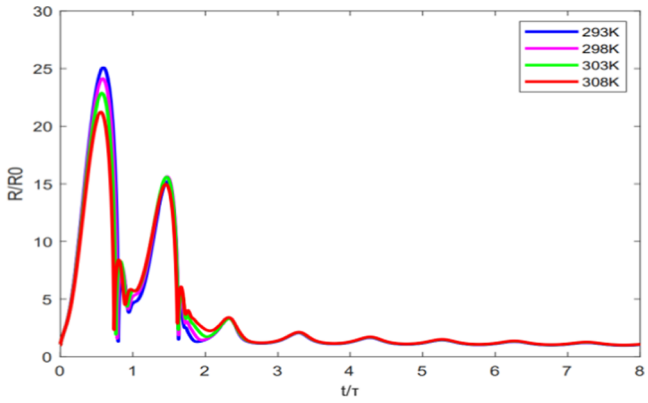

Figure 5. Variation curve of the cavitation bubble radius ratio with dimensionless time at different liquid temperatures. (T = 293, 298, 303, and 308 K; R_0 = 50 μm; P_1 = 0.5 MPa; P_2 = 0.1 MPa; C = 0.2 wt %; d_0 = 9 mm; and d_p = 25 mm).

The simulation results show that the number of water molecules in the cavitation bubble increased, but the maximum radius ratio, collapse pressure, and collapse temperature of the cavitation bubble decreased with the increase of the solution temperature. The physical properties of the solution, such as density, viscosity, surface tension, and saturated vapor pressure, changed with the increase of the solution temperature. With the increase of the saturated vapor pressure and the number density of water molecules at the cavitation bubble wall, the number of water molecules diffused into the cavitation bubble increased. On the other hand, with the increase of the liquid temperature, the surface tension decreased, which led to the decrease of the collapse pressure and collapse temperature. Compared with the increase of the number of water molecules, the decrease of the collapse pressure and temperature has a greater influence on the yield of free radicals. Therefore, the

Table 4. Collapse Pressure, Collapse Temperature, Water Molecular Number, and •OH Yield in the Cavitation Bubble under Different Liquid Concentrations

concentration of the chitosan solution/wt %	collapse pressure/Pa	collapse temperature/K	molecular number of water (N_w)	hydroxyl radical/mol
pure water	2.10×10^7	2232.86	2.55×10^{15}	8.48×10^{-12}
0.2	4.94×10^6	1630.16	8.18×10^{14}	1.15×10^{-12}
0.4	3.60×10^6	1523.15	7.18×10^{14}	7.21×10^{-13}
0.6	8.24×10^5	1092.55	4.60×10^{14}	5.08×10^{-14}

https://dx.doi.org/10.1021/acsomega.0c05335
ACS Omega 2021, 6, 3736−3744

Table 5. Collapse Pressure, Collapse Temperature, Water Molecular Number, and •OH Yield in the Cavitation Bubble at Different Liquid Temperatures

solution temperature/K	collapse pressure/Pa	collapse temperature/K	molecular number of water (N_w)	hydroxyl radical/mol
293	1.33×10^7	2018.03	5.69×10^{14}	2.27×10^{-12}
298	8.35×10^6	1829.05	6.99×10^{14}	1.98×10^{-12}
303	4.94×10^6	1630.16	8.18×10^{14}	1.15×10^{-12}
308	2.66×10^6	1414.96	9.14×10^{14}	5.49×10^{-13}

increase of the solution temperature led to the decrease of the •OH yield, which was consistent with the experimental results.[36,37]

3.5. Effect of the Initial Radius of the Cavitation Bubble. Under the conditions of T_0 = 303 K, C = 0.2 wt %, P_1 = 0.5 MPa, P_2 = 0.1 MPa, d_0 = 9 mm, and d_p = 25 mm, the influence of the initial cavitation bubble radius (50, 70, 90, 110, and 130 μm) on the •OH yield was investigated. The results are shown in Figure 6 and Table 6.

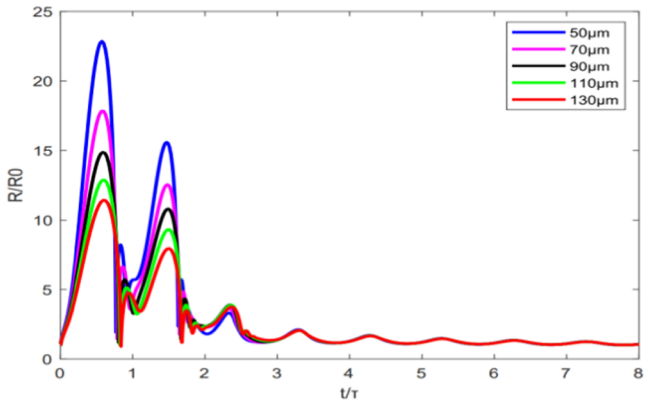

Figure 6. Variation curve of the cavitation bubble radius ratio with dimensionless time under different initial cavitation bubble radii. (R_0 = 30, 50, 70, 90, and 100 μm; T_0 = 303 K; C = 0.2 wt %; P_1 = 0.5 MPa; P_2 = 0.1 MPa; d_0 = 9 mm; and d_p = 25 mm).

Table 6. Collapse Pressure, Collapse Temperature, Water Molecular Number, and •OH Yield in the Cavitation Bubble at Different Initial Cavitation Bubble Radii

initial radius/μm	collapse pressure/Pa	collapse temperature/K	molecular number of water (N_w)	hydroxyl radical/mol
50	4.94×10^6	1630.16	8.18×10^{14}	1.15×10^{-12}
70	5.93×10^6	1720.69	1.03×10^{15}	1.83×10^{-12}
90	6.56×10^6	1787.25	1.24×10^{15}	2.46×10^{-12}
110	6.87×10^6	1840.78	1.44×10^{15}	3.26×10^{-12}
130	6.90×10^6	1885.70	1.63×10^{15}	3.82×10^{-12}

Figure 6 and Table 6 show that with the increase of the initial radius of the bubble, the maximum radius of the bubble increased, the collapse pressure and collapse temperature of the cavity increased, and the number of water molecules evaporated into the bubble increased. Consequently, the production of free radicals increased. In addition, the cavitation intensity was positively correlated with the maximum radius of the cavitation bubble, so the collapse intensity of the cavitation bubble increased with the increase of the maximum radius. Under the influence of the above factors, the decomposition rate of water vapor in the cavitation bubble accelerated and the amount of •OH increased, which was consistent with the experimental results.[38]

3.6. Effect of the Pipe Diameter Downstream of the Orifice Plate. Under the conditions of T_0 = 303 K, R_0 = 100 μm, C = 0.2 wt %, P_1 = 0.5 MPa, P_2 = 0.1 MPa, and the constant ratio of the orifice diameter to the pipe diameter (β), the influence of the pipe diameter d_p (25, 50, 75, and 100 mm) on the •OH yield was investigated.

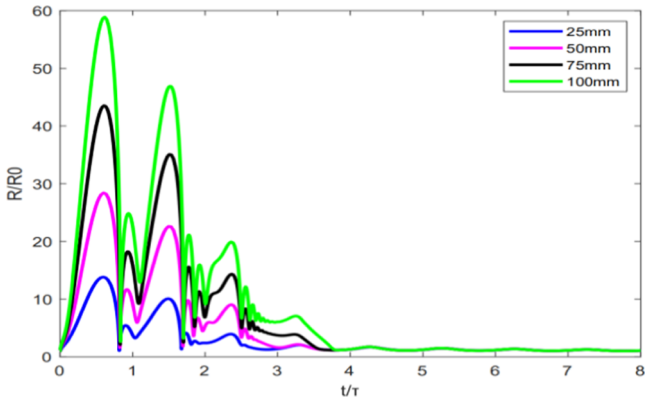

Figure 7. Variation curve of the cavitation bubble radius ratio with dimensionless time under different pipe diameters. (d_p = 25, 50, 75, and 100 mm; T_0 = 303 K; R_0 = 100 μm; C = 0.2 wt %; P_1 = 0.5 MPa; and P_2 = 0.1 MPa).

Figure 7 and Table 7 show that the maximum radius ratio, collapse pressure, and collapse temperature increased with the increase of the diameters of the orifice plate and the downstream pipe. Correspondingly, with the increase of the diameters of the orifice and the pipe, the turbulence scale became larger and the pulsation frequency of the turbulence was reduced so that the cavitation bubble can fully grow. The larger the maximum radius of the cavitation bubble, the stronger the turbulence. Consequently, the collapse effect could be better. In addition, the movement of the cavitation bubble was affected by both radial flow and turbulent pulsation. With the increase of d_p, the radial pressure gradient decreased, and the turbulent pulsating pressure was the main driving force of the cavitation bubble movement. Therefore, under the condition of constant β, the larger the diameter of the pipe downstream of the orifice plate, the higher the cavitation intensity and the higher the production of •OH.[31]

3.7. Influence of the Ratio of the Orifice Diameter to the Pipe Diameter (β). Under the conditions of C = 0.2 wt %, T_0 = 303 K, R_0 = 100 μm, P_1 = 0.5 MPa, P_2 = 0.1 MPa, and d_p = 25 mm, the influence of the ratio of the orifice diameter to the pipe diameter (β) (0.2, 0.24, 0.28, 0.32, 0.36) on the •OH yield was investigated. The results are shown in Figure 8 and Table 8.

The results show that with the increase of the ratio of the orifice diameter to the pipe diameter (β), the turbulent pulsation frequency decreased, but the maximum radius ratio,

https://dx.doi.org/10.1021/acsomega.0c05335
ACS Omega 2021, 6, 3736−3744

Table 7. Collapse Pressure, Collapse Temperature, Water Molecular Number, and •OH Yield in the Cavitation Bubble with Different Pipe Diameters

hole diameter of the orifice plate/mm	pipe diameter downstream of the orifice plate/mm	collapse pressure/Pa	collapse temperature/K	molecular number of water (N_w)	hydroxyl radical/mol
9	25	6.78×10^{6}	1817.55	1.33×10^{15}	2.89×10^{-12}
18	50	1.71×10^{7}	2255.08	8.89×10^{15}	1.91×10^{-11}
27	75	2.35×10^{7}	2459.52	2.76×10^{16}	4.40×10^{-11}
36	100	2.84×10^{7}	2598.03	6.13×10^{16}	7.81×10^{-11}

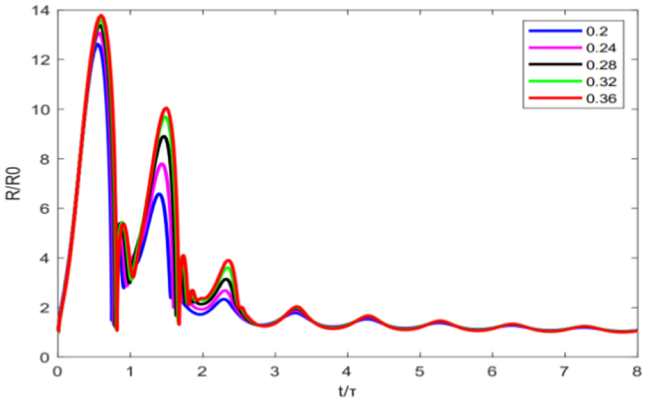

Figure 8. Variation curve of the cavitation bubble radius ratio with dimensionless time under different orifice diameter to pipe diameter ratios. (β = 0.2, 0.24, 0.28, 0.32, 0.36; C = 0.2 wt %; T_0 = 303 K; R_0 = 100 μm; P_1 = 0.5 MPa; P_2 = 0.1 MPa; and d_p = 25 mm).

Table 8. Collapse Pressure, Collapse Temperature, Water Molecular Number, and •OH Yield in the Cavitation Bubble with Different Pore Diameter to Pipe Diameter Ratios

ratio of the orifice diameter to the pipe diameter (β)	collapse pressure/Pa	collapse temperature/K	molecular number of water (N_w)	hydroxyl radical/mol
0.20	1.76×10^{6}	1346.34	1.22×10^{15}	9.17×10^{-13}
0.24	2.84×10^{6}	1501.82	1.27×10^{15}	1.06×10^{-12}
0.28	4.01×10^{6}	1620.49	1.31×10^{15}	1.59×10^{-12}
0.32	5.23×10^{6}	1716.90	1.33×10^{15}	2.19×10^{-12}
0.36	6.78×10^{6}	1817.55	1.34×10^{15}	2.89×10^{-12}

collapse pressure, and collapse temperature of the bubbles increased. Not only the decomposition rate of water vapor in the cavitation bubble accelerated but also the yield of •OH increased when the collapse strength of the cavitation bubble and the number of water molecules in the cavitation bubble increased. In addition, when β was greater than 0.36, choking cavitation occurred. This was consistent with the experimental studies.[35,39,40]

4. CONCLUSIONS

In this work, the hydrodynamic cavitation process based on orifice plates was studied by a numerical simulation. The influence of different factors on the yield of •OH was investigated. The increase of the upstream inlet pressure led to the larger flow field pressure gradient and turbulence intensity, which made the cavitation bubble expansion and collapse more intense, so the yield of •OH increased up to an optimal inlet pressure. The increase in the recovery pressure downstream of the orifice led to more adequate growth of the cavitation bubble, greater turbulence intensity, and more violent collapse, so the yield of •OH increased. As the concentration and viscosity of the chitosan solution increased, liquid properties such as saturated vapor pressure, surface tension, and specific heat capacity decreased and the •OH yield was reduced. With the increase of the liquid temperature, the viscosity of the liquid decreased and the saturated vapor pressure of the solution increased, which led to the decrease of the cavitation bubble collapse strength and was not conducive to the formation of hydroxyl radicals. The increase of the initial radius of the cavitation bubble resulted in the enhancement of the turbulent pulsating pressure effect, the stronger cavitation bubble collapse intensity, and the increase of the yield of •OH. In the case of constant β, the cavitation strength and the •OH yield increased by increasing the diameter of the pipe downstream of the orifice. With the increase of β, the cavitation bubble collapse strength and the yield of •OH increased, and the effect was best when β = 0.36. Choking cavitation occurred when β > 0.36.

This work provided a numerical simulation method for the study of the hydroxyl radical yield in a hydrodynamic cavitation bubble of a chitosan solution. The simulation results provided a basis for further research on the •OH yield and process optimization of the hydrodynamic cavitation of the chitosan solution.

AUTHOR INFORMATION

Corresponding Author

Yongchun Huang − *Guangxi Key Laboratory of Green Processing of Sugar Resources, Guangxi University of Science and Technology, Liuzhou 545006, Guangxi, P. R. China; School of Biological and Chemical Engineering, Guangxi University of Science and Technology, Liuzhou 545006, Guangxi, P. R. China;* orcid.org/0000-0003-0637-3791; Email: huangyc@yeah.net

Authors

Xiangyu Zhang − *Guangxi Key Laboratory of Green Processing of Sugar Resources, Guangxi University of Science and Technology, Liuzhou 545006, Guangxi, P. R. China; School of Biological and Chemical Engineering, Guangxi University of Science and Technology, Liuzhou 545006, Guangxi, P. R. China;* orcid.org/0000-0003-2335-1623

Xinfeng Zhu − *Guangxi Key Laboratory of Green Processing of Sugar Resources, Guangxi University of Science and Technology, Liuzhou 545006, Guangxi, P. R. China; School of Biological and Chemical Engineering, Guangxi University of Science and Technology, Liuzhou 545006, Guangxi, P. R. China*

Yan Cao − *Guangxi Key Laboratory of Green Processing of Sugar Resources, Guangxi University of Science and Technology, Liuzhou 545006, Guangxi, P. R. China; School of Biological and Chemical Engineering, Guangxi University of Science and Technology, Liuzhou 545006, Guangxi, P. R. China*

https://dx.doi.org/10.1021/acsomega.0c05335
ACS Omega 2021, 6, 3736−3744

Kunming Zhang − *Guangxi Key Laboratory of Green Processing of Sugar Resources, Guangxi University of Science and Technology, Liuzhou 545006, Guangxi, P. R. China; School of Biological and Chemical Engineering, Guangxi University of Science and Technology, Liuzhou 545006, Guangxi, P. R. China*

Feng Yang − *Guangxi Key Laboratory of Green Processing of Sugar Resources, Guangxi University of Science and Technology, Liuzhou 545006, Guangxi, P. R. China; School of Biological and Chemical Engineering, Guangxi University of Science and Technology, Liuzhou 545006, Guangxi, P. R. China*

Xian'e Ren − *Guangxi Key Laboratory of Green Processing of Sugar Resources, Guangxi University of Science and Technology, Liuzhou 545006, Guangxi, P. R. China; School of Biological and Chemical Engineering, Guangxi University of Science and Technology, Liuzhou 545006, Guangxi, P. R. China*

Complete contact information is available at: https://pubs.acs.org/10.1021/acsomega.0c05335

Notes

The authors declare no competing financial interest.

■ ACKNOWLEDGMENTS

This work was supported by the National Natural Science Foundation of China (No. 31660472).

■ REFERENCES

(1) Ravi Kumar, M. N. V.; Muzzarelli, R. A. A.; Muzzarelli, C.; Sashiwa, H.; Domb, A. J. , Chitosan chemistry and pharmaceutical perspectives. *Chem. Rev.* **2004**, *104*, 6017−6084.

(2) Bakshi, P. S.; Selvakumar, D.; Kadirvelu, K.; Kumar, N. S. Chitosan as an environment friendly biomaterial - a review on recent modifications and applications. *Int. J. Biol. Macromol.* **2020**, *150*, 1072−1083.

(3) Cabrera, J. C.; Van Cutsem, P. Preparation of chitooligosaccharides with degree of polymerization higher than 6 by acid or enzymatic degradation of chitosan. *Biochem. Eng. J.* **2005**, *25*, 165−172.

(4) Czechowska-Biskup, R.; Rokita, B.; Lotfy, S.; Ulanski, P.; Rosiak, J. M. Degradation of chitosan and starch by 360-kHz ultrasound. *Carbohydr. Polym.* **2005**, *60*, 175−184.

(5) Wasikiewicz, J. M.; Yoshii, F.; Nagasawa, N.; Wach, R. A.; Mitomo, H. Degradation of chitosan and sodium alginate by gamma radiation, sonochemical and ultraviolet methods. *Radiat. Phys. Chem.* **2005**, *73*, 287−295.

(6) Zhi, L. Study on γ-Ray Irradiation Degradation of Chitosan. *Chin. J. Appl. Chem.* **2001**.

(7) Huang, Y.; Wu, Y.; Huang, W.; Yang, F.; Ren, X. Degradation of chitosan by hydrodynamic cavitation. *Polym. Degrad. Stab.* **2013**, *98*, 37−43.

(8) Wu, Y.; Huang, Y.; Zhou, Y.; Ren, X.; Yang, F. Degradation of chitosan by swirling cavitation. *Innovative Food Sci. Emerging Technol.* **2014**, *23*, 188−193.

(9) Huang, Y.; Wang, P.; Yuan, Y.; Ren, X.; Yang, F. Synergistic degradation of chitosan by impinging stream and jet cavitation. *Ultrason. Sonochem.* **2015**, *27*, 592−601.

(10) Yan, J.; Ai, S.; Yang, F.; Zhang, K.; Huang, Y. Study on mechanism of chitosan degradation with hydrodynamic cavitation. *Ultrason. Sonochem.* **2020**, *64*, No. 105046.

(11) Yan, J.; Xu, J.; Ai, S.; Zhang, K.; Yang, F.; Huang, Y. Degradation of chitosan with self-resonating cavitation. *Arabian J. Chem.* **2020**, *13*, 5776−5787.

(12) Storey, B. D.; Szeri, A. J. Water vapour, sonoluminescence and sonochemistry. *Proc. R. Soc. London, Ser. A* **2000**, *456*, 1685−1709.

(13) Yasui, K.; Tuziuti, T.; Sivakumar, M.; Iida, Y. Theoretical study of single-bubble sonochemistry. *J. Chem. Phys.* **2005**, *122*, No. 224706.

(14) J. Sangeeth Krishnan, P. D.; Vijayanand, S. M. Numerical Investigation into the Chemistry Induced by Hydrodynamic Cavitation. *Ind. Eng. Chem. Res.* **2006**, *45*, 1493−1504.

(15) Kumar, P.; Moholkar, V. S. Numerical Assessment of Hydrodynamic Cavitation Reactors Using Organic Solvents. *Ind. Eng. Chem. Res.* **2011**, *50*, 4769−4775.

(16) Rajoriya, S.; Bargole, S.; Saharan, V. K. Degradation of a cationic dye (Rhodamine 6G) using hydrodynamic cavitation coupled with other oxidative agents: Reaction mechanism and pathway. *Ultrason. Sonochem.* **2017**, *34*, 183−194.

(17) Chokradjaroen, C.; Theeramunkong, S.; Yui, H.; Saito, N.; Rujiravanit, R. Cytotoxicity against cancer cells of chitosan oligosaccharides prepared from chitosan powder degraded by electrical discharge plasma. *Carbohydr. Polym.* **2018**, *201*, 20−30.

(18) Gilmore, F. R. *The Growth or Collapse of a Spherical Bubble in a Viscous Compressible Liquid*; California Institute of Technology: Pasadena, 1952.

(19) Yan, Y.; Thorpe, R. B. Flow regime transitions due to cavitation in the flow through an orifice. *Int. J. Multiphase Flow* **1990**, *16*, 1023−1045.

(20) Abdulaziz, A. M. Performance and image analysis of a cavitating process in a small type venturi. *Exp. Therm. Fluid Sci.* **2014**, *53*, No. 40.

(21) Tao, Y.; Cai, J.; Huai, X.; Liu, B. Global Average Hydroxyl Radical Yield throughout the Lifetime of Cavitation Bubbles. *Chem. Eng. Technol.* **2018**, *41*, 1035−1042.

(22) Nurick, W. H. Orifice Cavitation and Its Effect on Spray Mixing. *J. Fluids Eng.* **1976**, *98*, No. 681.

(23) Mishra, C.; Peles, Y. Size scale effects on cavitating flows through microorifices entrenched in rectangular microchannels. *J. Microelectromech. Syst.* **2005**, *14*, 987−999.

(24) Payri, R.; Salvador, F. J.; Gimeno, J.; de la Morena, J. Study of cavitation phenomena based on a technique for visualizing bubbles in a liquid pressurized chamber. *Int. J. Heat Fluid Flow* **2009**, *30*, 768−777.

(25) Mishra, C.; Peles, Y. Cavitation in flow through a micro-orifice inside a silicon microchannel. *Phys. Fluids* **2005**, *17*, No. 013601.

(26) Mancuso, G.; Langone, M.; Andreottola, G. A critical review of the current technologies in wastewater treatment plants by using hydrodynamic cavitation process: principles and applications. *J. Environ. Health Sci. Eng.* **2020**, *18*, 311−333.

(27) Xu, S.; Wang, J.; Cheng, H.; Ji, B.; Long, X. Experimental study of the cavitation noise and vibration induced by the choked flow in a Venturi reactor. *Ultrason. Sonochem.* **2020**, *67*, No. 105183.

(28) Toegel, R.; Gompf, B.; Pecha, R.; Lohse, D. Does water vapor prevent upscaling sonoluminescence? *Phys. Rev. Lett.* **2000**, *85*, 3165−3168.

(29) Sivasankar, T.; Paunikar, A. W.; Moholkar, V. S. Mechanistic approach to enhancement of the yield of a sonochemical reaction. *AIChE J.* **2007**, *53*, 1132−1143.

(30) Sivasankar, T.; Moholkar, V. S. Physical insights into the sonochemical degradation of recalcitrant organic pollutants with cavitation bubble dynamics. *Ultrason. Sonochem.* **2009**, *16*, 769−781.

(31) Cai, J.; XiuLan, H.; XunFeng, L. I. Investigation on cavitation bubble dynamics in compressible liquid under turbulence. *Chin. Sci. Bull.* **2010**, *55*, 857−866.

(32) Yasui, K.; Tuziuti, T.; Iida, Y. Optimum bubble temperature for the sonochemical production of oxidants. *Ultrasonics* **2004**, *42*, 579−584.

(33) Torabi Angaji, M.; Ghiaee, R. Decontamination of unsymmetrical dimethylhydrazine waste water by hydrodynamic cavitation-induced advanced Fenton process. *Ultrason. Sonochem.* **2015**, *23*, 257−265.

(34) Nilesh, P.; Vichare, P. R. G.; Aniruddha, B. P. Optimization of Hydrodynamic Cavitation Using a Model Reaction. *Chem. Eng. Technol.* **2000**, *23*, 683−690.

(35) Braeutigam, P.; Franke, M.; Wu, Z. L.; Ondruschka, B. Role of Different Parameters in the Optimization of Hydrodynamic Cavitation. *Chem. Eng. Technol.* **2010**, *33*, 932−940.
(36) Chakinalaa, A. G.; Gogate, P. R.; Burgess, A. E.; Bremner, D. H. Industrial wastewater treatment using hydrodynamic cavitation and heterogeneous advanced Fenton processing. *Chem. Eng. J.* **2009**, *152*, 498−502.
(37) Tao, Y.; Cai, J.; Huai, X.; Liu, B.; Guo, Z. Application of Hydrodynamic Cavitation to Wastewater Treatment. *Chem. Eng. Technol.* **2016**, *39*, 1363−1376.
(38) Capocelli, M.; Prisciandaro, M.; Lancia, A.; Musmarra, D. Hydrodynamic cavitation of p-nitrophenol: A theoretical and experimental insight. *Chem. Eng. J.* **2014**, *254*, 1−8.
(39) Parag, R.; Gogate, A. B. P. Engineering Design Methods for Cavitation Reactors II: Hydrodynamic Cavitation. *AIChE J.* **2000**, *46*, 1641−1649.
(40) Sharma, A.; Gogate, P. R.; Mahulkar, A.; Pandit, A. B. Modeling of hydrodynamic cavitation reactors based on orifice plates considering hydrodynamics and chemical reactions occurring in bubble. *Chem. Eng. J.* **2008**, *143*, 201−209.

https://dx.doi.org/10.1021/acsomega.0c05335
ACS Omega 2021, 6, 3736−3744